Acta Cryst. (1994). D**50**, 385–395

Light-Scattering Investigations of Nucleation Processes and Kinetics of Crystallization in Macromolecular Systems

BY ALEXANDER J. MALKIN AND ALEXANDER MCPHERSON

Biochemistry Department, University of California, Riverside, CA 92521, *USA*

(*Received* 10 *September* 1993; *accepted* 26 *November* 1993)

Abstract

Quasi-elastic light scattering (QELS) was used to investigate quantitatively the mechanisms of nucleation, postnucleation growth, and dissolution in ensembles of both crystalline and amorphous aggregates of satellite tobacco mosaic virus (STMV), ferritin, apoferritin and pumpkin seed globulin. At low supersaturation conditions, as described previously for small molecule crystallization, the metastable region was obtained. Under these conditions aggregation took place, but crystallization did not proceed and critical nuclei did not form over a long period of time. The critical solution supersaturation necessary to obtain crystals, $\sigma = \ln(c/s)$ where c and s are concentration and solubility of protein, varied from ~ 0.1 for pumpkin seed globulin to ~ 0.9 for STMV. For higher supersaturation conditions when aggregation processes leading to formation of crystals are not established immediately but after a certain induction period, the supersaturation-dependent critical nuclear size, R_c, for different macromolecular systems was estimated from time-dependent size-distribution analyses to be in the range of $\sim 10^3$ for proteins such as pumpkin globulin to approximately 10 for virus particles. From the same data, the molar interfacial free energy was deduced to be 3.3–9.2 kJ mol^{-1}. These are believed to be among the first estimates for macromolecular crystals. Under conditions of moderate supersaturation where induction periods preceded the appearance of critical nuclei, the potential barriers for formation were estimated to be in the range 8.3–50 kJ mol^{-1}. Growth and dissolution kinetics for pumpkin seed globulin were investigated. These experiments allowed determination of protein solubility *versus* solution temperature, protein and precipitant concentrations. Aggregation patterns which lead to crystal formation are distinctly different to those which produce an amorphous precipitate. The results provide additional evidence that QELS can be used to find general criteria that allow one to discriminate between conditions for a given protein system leading to crystalline or amorphous states at early stages of the aggregation process.

1. Introduction

There is no longer a need to underline the importance of fundamental investigations in macromolecular crystal growth. It has become apparent that lack of understanding of the processes which take place in protein crystal growth prevents the development of new effective crystal growth techniques.

Among the most important problems in macromolecular crystal growth are qualitative and quantitative descriptions of nucleation phenomena which ultimately lead to the formation of a new crystalline phase. The best technique discovered so far for the investigations of nucleation phenomena appears to be quasi-elastic light scattering (QELS). This has been applied to the investigation of crystallization for different macromolecular systems (for reviews, see Wilson, 1990; Kam, Shore & Feher, 1978; Carter, Baldwin & Frick, 1988; Bishop, Fredericks, Howard & Sawada, 1992; Kadima, McPherson, Dunn & Jurnak, 1991; Lorber, Skouri, Munch & Giegé, 1993; Mikol, Hirsh & Giegé, 1990). We recently applied QELS to the investigation of nucleation and crystallization phenomena in several large macromolecular assemblies that included satellite tobacco mosaic virus (STMV), apoferritin, ferritin and pumpkin seed globulin (Malkin, Cheung & McPherson, 1993; Malkin & McPherson, 1993*a*,*b*,*c*). In doing so, we were able to obtain supersaturation dependencies for the size of the critical nuclei which will support crystal growth, and determine quantitatively such fundamental crystal growth parameters as interfacial free energies and crystallization activation energies. The considerable differences in the aggregation pathways leading both to crystals and an amorphous precipitate were obtained. For pumpkin seed globulin, the solubility of which has a strong temperature dependence, both aggregation and dissociation kinetics were investigated. This allowed us to obtain solubility data as a function of precipitant concentration and temperature.

It should be noted that our major efforts were concentrated on the investigation of crystallization of satellite tobacco mosaic virus. We believe that STMV is one of the best model systems for protein

crystal growth investigations. Its three-dimensional structure was recently solved to 2.9 Å resolution (Larson, Koszelak, Day, Greenwood & McPherson, 1993*a*,*b*). It is easily and reproducibly crystallized using a variety of precipitation agents. STMV crystals are very stable both mechanically and chemically. The virus is very close to spherical, thus it follows classical crystal growth theories well. It is a large 16 nm particle and hence it produces strong and unambiguous light-scattering signals as it forms aggregates of different sizes through the crystallization process.

2. Experimental

2.1. *Materials*

STMV (molecular weight $\simeq$ 1 500 000 Da) was purified from co-infected TMV tobacco plants as described by Valverde & Dodds (1987). Isolation and crystallization of pumpkin seed globulin (molecular weight $\simeq$ 112 000 Da) was based on the method of Hara, Wada, Wakabayashi & Matsubara (1976). Horse spleen ferritin (molecular weight $\simeq$ 443 000 Da) was purchased from Sigma Co. (St Louis, Missouri, USA). Apoferritin was prepared from ferritin as described by Treffry & Harrison (1978).

STMV, ferritin and apoferritin crystals could be obtained simply by mixing protein dissolved in water directly with the appropriate precipitant [0.5–1% $CdSO_4$ for ferritin and apoferritin and a variety of precipitants (see §3.2.2) for STMV]. Supersaturation conditions for pumpkin globulin crystallization were created by decreasing the solution temperature below the equilibrium temperature T_{eq}.

2.2 *Methods*

Light-scattering measurements were made in photon-correlation mode (Berne & Pecora, 1976; Pecora, 1985) using a Malvern 4700c submicro particle analyzer. The exponential sampling method (Cummins & Staples, 1987) was utilized in order to produce particle-size-distribution (PSD) data. The size-distribution data were calculated as a set of 24 discrete entities by the fitting of the intensity correlation function to a family of exponential functions. Average sizes of the aggregates were estimated from distributions of mass. Instruments and methods were carefully calibrated with sphere standards and mixtures of such standards (Malkin, Cheung & McPherson, 1993).

Special precautions in sample preparation were taken, including centrifugation at 12000*g* for $\sim$30 min and filtration through 0.22 μm syringe filters for all protein and precipitant solutions in order to remove dust particles which could affect measurements. Samples had total volumes of 100–120 μl and were maintained through measurements at 295 (0.1) K. For the investigation of the temperature-dependent aggregation and dissociation kinetics of the pumpkin seed globulin, data were obtained in the 277–328 K temperature range.

Solution supersaturation σ was determined as $\sigma = \ln(c/s)$, where c and s are the concentration and solubility of the protein solution, respectively. Solubilities, s, were obtained by measuring supernatant protein concentrations in cells in which crystal growth was complete, usually after approximately 1 month. All experimental details were the same as described earlier (Malkin, Cheung & McPherson, 1993) and will not be repeated here.

3. Results and discussion

Aggregation phenomena leading to the formation of the critical crystalline nuclei and further postnucleation growth for STMV, apoferritin and pumpkin seed globulin crystals were investigated in a wide supersaturation range. Even in protein solutions lacking precipitant aggregation took place resulting in the appearance of small approximately 3–10-monomer clusters (§3.1).

At low supersaturations we were able to identify conditions where critical nuclei were not formed for a long period of time. These conditions were viewed as those corresponding to the metastable region (§3.2.1).

For all protein and virus systems investigated in this work, the supersaturation range was obtained where the continuous aggregation process leading to the appearance of the crystalline phase did not become established immediately but only after a certain induction period necessary for the formation of critical nuclei (§3.2.2). This allowed us to obtain the supersaturation dependencies of the critical nuclei and estimate interfacial free energies between the crystalline nucleus and bulk solution. At higher supersaturations aggregation proceeded immediately and crystals appeared shortly after incubation of protein solution with precipitant (§3.2.2).

For the pumpkin seed globulin we investigated the temperature-dependent aggregation and dissolution processes, which allowed us to obtain the solubility data as a function of precipitant concentration and temperature (§3.2.3).

The differences in the aggregation pathways leading both to the amorphous precipitate and crystals will be discussed in §3.2.4.

3.1. *Unsaturated protein and virus solutions*

For STMV, apoferritin and ferritin dissolved in water, two peaks were usually present in the PSD.

For STMV solutions the major component in the PSD corresponded to 16–17 nm, while those for apoferritin and ferritin were in range 11–12 nm. These correspond exactly to the molecular diameters for STMV, ferritin and apoferritin as based on X-ray (Harrison, 1959; Koszelak, Dodds & McPherson, 1989) and electron microscopy (Valverde & Dodds, 1987) results. Aggregation took place even in the solutions lacking precipitant and small 2–10-mer clusters with sizes in the range 19–30 nm in the case of STMV and 14–22 nm for apoferritin and ferritin were present in the PSD data. These clusters do not usually exceed 3–5% by mass of the total particles in solution.

So far, we have had only one batch of highly monodisperse STMV solutions where no aggregation took place. In this case only 16–17 nm STMV monomers were present in the solutions. Surprisingly, when incubations contained the same precipitating agents for monodisperse STMV solutions and those STMV solutions that contained 2–10-mer clusters, the aggregation pathways were completely different (§3.2.4).

In the undersaturated pumpkin globulin solutions the major species in the PSD corresponded to 5–6 nm, usually accompanied by clusters with sizes in the range 8–15 nm. Currently, there are no X-ray diffraction or other physical data on pumpkin globulin crystals. Thus, the size of the pumpkin globulin monomer was unclear. We assume from our QELS data that it corresponds to 5–6 nm. This appeared to be consistent with a reported molecular weight of 112000 Da (Hara *et al.*, 1976).

3.2. *Supersaturated solutions*

The solubility curve divides the whole region of the phase diagram into unsaturated and supersaturated zones (Fig. 1). The supersaturated zone is known to be divided into labile and metastable regions. In the labile region the driving force of the crystallization process – solution supersaturation – is enough for the nucleation process to take place and for further crystal growth. At lower supersaturations, corresponding to the metastable region, critical nuclei could not form for a long period of time.

The free energy, δF, for formation of a spherical crystalline aggregate of radius r is (Chernov, 1984)

$$\delta F = -4\pi r^3 kT\sigma/3\Omega + 4\pi r^2\alpha, \qquad (1)$$

where Ω is the volume of protein monomer in the crystal, σ is the solution supersaturation, k is the Boltzman constant, and α is the interfacial free energy between a crystal nucleus and the bulk solution.

The interfacial free energy represents the amount of work that it is necessary to supply in order to create a unit of surface of the new crystalline face. A measure of the interfacial free energy for the different macromolecular systems is essential for the quantitative description of the macromolecular crystal growth, since it is utilized in a number of equations describing both nucleation and kinetics of crystal growth.

Dependencies of the free energy δF *versus* size of the aggregate for different values of solution supersaturation σ are shown in Fig. 2. In order to form critical nuclei of size

$$R_c = 4\Omega\alpha/kT\sigma, \qquad (2)$$

it is necessary to overcome a potential barrier δF_c,

$$\delta F_c = 16\pi\Omega^2\alpha^3/3(kT\sigma)^2. \qquad (3)$$

Aggregates with the size $R < R_c$ are unstable and dissociate, since dissociation proceeds with a gain in energy (Fig. 2). If the size of critical nuclei, R_c,

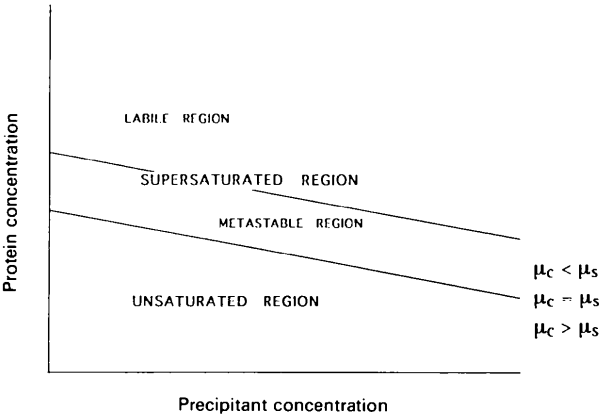

Fig. 1. Typical solubility diagram: μ_c and μ_s are the chemical potentials of the protein molecule in crystal and solution, respectively.

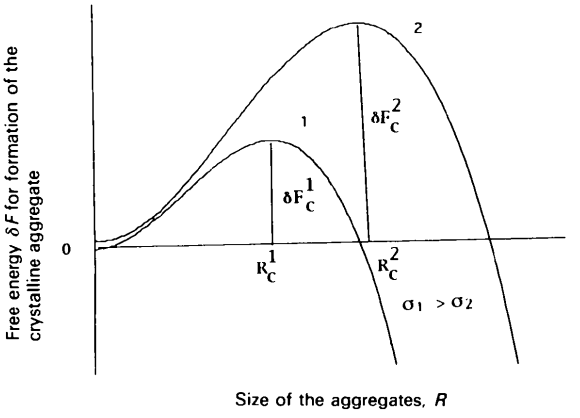

Fig. 2. Free energy, δF, of formation of an embryo of a new crystalline phase for the different supersaturation conditions $\sigma_1 > \sigma_2$.

increases, the aggregate will continue to grow (Fig. 2) and form a macroscopic new phase. Minor fluctuations in the size of aggregates when by some chance the size R becomes more than R_c result in irreversible growth (Fig. 2) and formation of a new macroscopic phase. Thus, actually, the energetics of formation of critical nuclei determine the energetics of the whole crystallization process.

3.2.1. *Metastable region.* Following on from (2) and (3) the size of critical nuclei and the activation barrier δF_c increases when solution supersaturation σ decreases. Thus, at a certain point fluctuations in free energy might not be enough to overcome the activation barrier δF_c and critical nuclei would not form even at the supersaturated conditions. This corresponds to the metastable region on the phase diagram (Fig. 1). The evaluation of the metastable conditions is important since they are supportive of crystal growth after the critical nuclei have already been formed. These also appear to be the optimal crystallization conditions, since usually for protein crystal growth excessive supersaturation conditions are used which are necessary for the formation of critical nuclei, and often result in the growth of poor quality crystals or microcrystals. As yet there appears to have been no reports describing metastable conditions for macromolecular systems.

Here we will describe aggregation in STMV solutions at supersaturations lower than those required for the crystallization. Later in §3.2.3 the metastable conditions for pumpkin globulin crystallization will also be described.

The potential barrier for formation of critical nuclei δF_c could, as follows from (3), be very high at low supersaturations. Thus, under these conditions we never obtained formation of critical nuclei, which ultimately resulted in a sharp increase in the aggregate sizes, followed by the appearance of visible microcrystals as discussed later in §3.2.2.

Thus, when 0.3–0.5 mg ml^{-1} STMV solutions were incubated with 0.1 M lithium sulfate, aggregates with average sizes in the range 28–35 nm, composed of ~5–10 virus particles, appeared in solution and existed over long periods of time (Fig. 3). Note that at the beginning ($t = 0$) of all experiments described in this paper, only monomers and small clusters (as described in §3.1) existed in the solutions. The average sizes of aggregates which appeared in solution (Fig. 3) were considerably larger than those with sizes in the range 19–30 nm (the average size being slightly higher than 20 nm) described in §3.1 for undersaturated conditions.

When higher concentrations of virus and precipitate were used (higher supersaturations σ), the system was driven more closely towards the labile region (Fig. 3). Larger aggregates with average sizes in the range 38–50 nm (1 mg ml^{-1} STMV incubated with 0.4 M Na,K tartrate) and 50–80 nm (0.5 mg ml^{-1} STMV with 0.25 M Li sulfate) appeared in the solutions (Fig. 3). Thus, the sizes of these relatively large aggregates composed of approximately 13–30 and 30–125 STMV monomers, respectively, were still smaller than those corresponding to the sizes of critical nuclei. A simple estimate for the size of critical nuclei for supersaturation below the critical level will be given later in §3.2.3.

As can be seen from Fig. 3, over long periods of time there was actually no increase in the aggregate sizes, which fluctuated with both aggregation and dissociation taking place. In about 2 months no visible crystals appeared in the solutions. These conditions were viewed as those corresponding to the metastable part of the supersaturation zone (Fig. 1).

3.2.2. *Non-stationary nucleation and size of the critical nucleus.* At supersaturation conditions higher than those described in §3.2.1, it was possible to distinguish clearly nuclei from the postnucleation aggregates. In the supersaturation regions $\sigma \simeq$ 1.0–1.4, 0.7–0.9 and 0.15–0.30 for STMV, apoferritin and pumpkin globulin crystallization, respectively, the aggregation process leading to the appearance of a new phase is not established immediately, but after a certain induction period t_{ind} required for the appearance of critical nuclei of size R_c (Figs. 4–6). This was based on the observation that when aggregates with sizes greater than R_c appeared (and the system overcame the potential barrier δF_c, shown in Fig. 2), irreversible aggregation took place and a

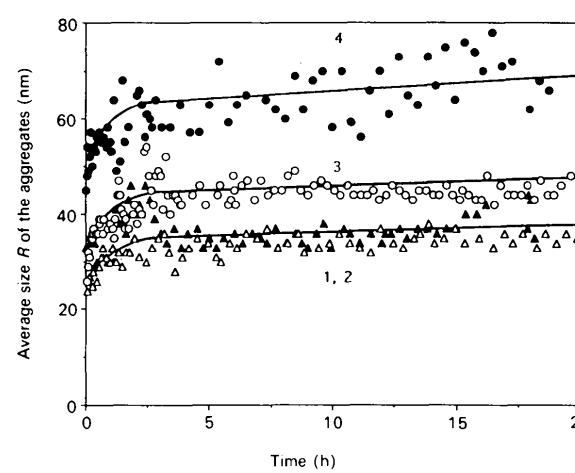

Fig. 3. The dependencies of the average sizes of aggregates R, formed under the creation of supersaturation conditions. (1) 0.3 mg ml^{-1} STMV incubated with 0.1 M Li sulfate; (2) 0.5 mg ml^{-1} STMV incubated with 0.1 M Li sulfate; (3) 1 mg ml^{-1} STMV incubated with 0.4 M Na,K tartrate; (4) 0.5 mg ml^{-1} STMV incubated with 0.25 M Li sulfate. Over long periods of time there was no actual increase in the aggregate sizes. No crystals were obtained under these supersaturations. These conditions were viewed as corresponding to the metastable zone.

sharp increase in the aggregate sizes up to μm sizes (Figs. 4–6) was obtained. The size of critical nuclei R_c was estimated as the greatest average size of aggregates that subsequently resulted in irreversible growth. This was followed by the appearance of microcrystals visible under a low-resolution microscope. During the induction period the size of aggregates with $R < R_c$ fluctuated, both dissociation and aggregation occurring, as described above in §3.2.1.

The duration of the induction period varied for different experiments, depending on the degree of solution supersaturation, from almost 5 h (Fig. 4*b*) to just 2–5 min (Fig. 5) at the higher supersaturation values.

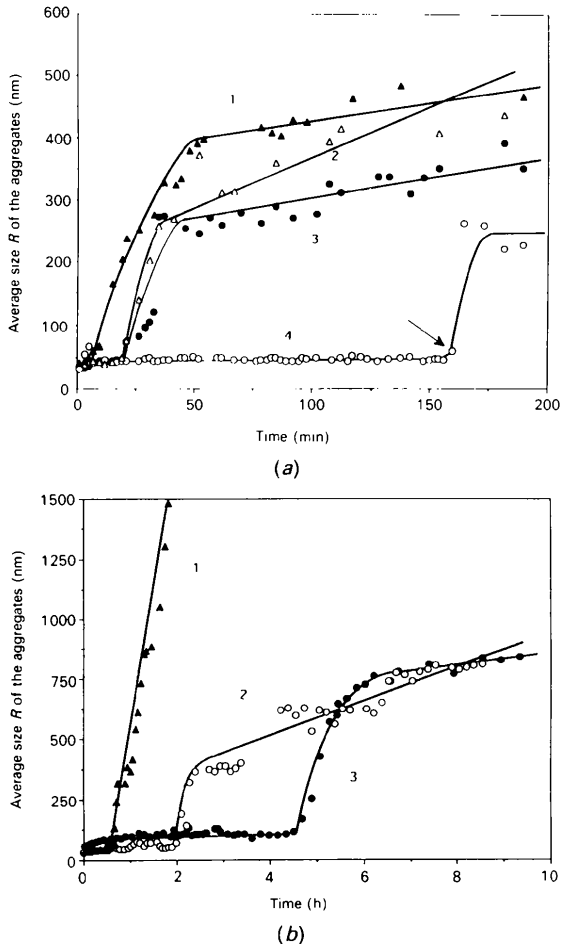

Fig. 4. Non-stationary nucleation when an induction period was required for the formation of critical nuclei. Time dependencies of the average sizes of the STMV aggregates $R(t)$ under different solution supersaturations. The precipitants used (*a*) 20% saturated ammonium sulfate. Supersaturations $\sigma \simeq$ (1) 1.25; (2) 1.15; (3) 1.05; (4) 1.0. In order to illustrate the procedure for the determination of the values for the critical nuclei, R_c, we indicated R_c in curve (4) with an arrow. (*b*) (1) 1 mg ml^{-1} STMV incubated with 1.0 *M* ammonium phosphate; (2) 2 mg ml^{-1} STMV incubated with 0.25 *M* Li sulfate; (3) 0.5 mg ml^{-1} STMV incubated with 0.35 *M* Li sulfate.

From our experimental data the sizes of critical nuclei R_c for STMV crystallization were estimated to be in the range 30–50 nm at supersaturation $\sigma \simeq 1.0$–1.4 (Fig. 7). They were composed of approximately 7–30 STMV monomers, respectively (Fig. 7, insert). For apoferritin crystallization (Fig. 7), values for R_c obtained experimentally were in the range from ~38–40 nm ($\sigma \simeq 0.92$) to ~50–52 nm ($\sigma \simeq 0.72$), and were composed of approximately 30–70 apoferritin monomers, respectively (Fig. 7, insert). For pumpkin globulin crystallization, the sizes of the critical nuclei R_c were estimated to range from 44–46 nm ($\sigma \simeq 0.3$) to 63–65 nm ($\sigma \simeq 0.18$). These corresponded to approximately 570–650 to 1.7–1.8 × 10^3 pumpkin molecules, respectively (Fig. 7).

From the supersaturation dependencies of the critical nuclei R_c obtained experimentally and according to (2) a further estimate could be made of the interfacial free energy α between a crystal

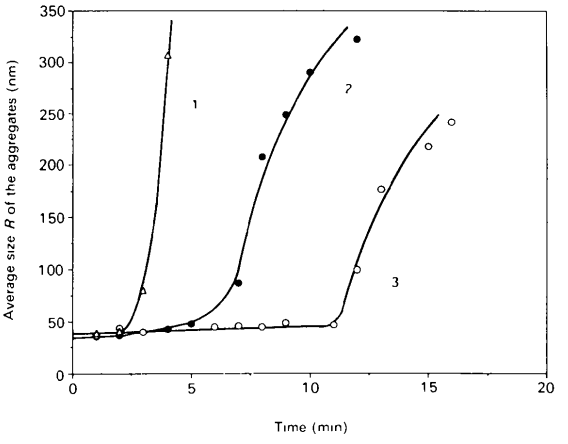

Fig. 5. Non-stationary apoferritin nucleation. Supersaturations $\sigma \simeq$ (1) 0.72; (2) 0.80; (3) 0.87; (4) 0.92.

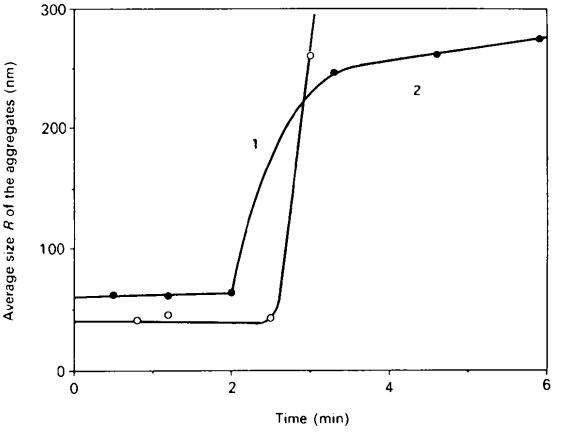

Fig. 6. Non-stationary pumpkin seed globulin nucleation. Supersaturations $\sigma \simeq$ (1) 0.30; (2) 0.18.

nucleus and bulk solution. With the values of $\Omega = 3.5 \times 10^{-18}$, 1.8×10^{-18} and 1.5×10^{-19} cm^3 for the volumes of STMV, apoferritin and pumpkin globulin monomers in the crystal, the values of α of 1.8×10^{-9} J cm^{-2} (molar free energy $\simeq 9.2$ kJ mol^{-1}) for the crystallization of STMV, 2.7×10^{-9} J cm^{-2} (molar free energy $\simeq 7.5$ kJ mol^{-1}) for apoferritin and 6.1×10^{-9} J cm^2 (molar free energy $\simeq 3.3$ kJ mol^{-1}) for pumpkin globulin were estimated from the experimental dependencies of R_c *versus* $1/\sigma$ (Fig. 7). The corresponding surface energies α/KT per virus and protein molecules are 3.7, 3.0 and 1.3 for STMV, apoferritin and pumpkin globulin, respectively. The comparable value of surface energy for a lysozyme molecule was estimated to be $\alpha/kT = 2.3$ (Durbin & Feher, 1990).

The values of the interfacial free energies for STMV, apoferritin and pumpkin globulin crystals estimated above are considerably lower than those for organic and inorganic crystals grown from the solutions. Thus, these values usually vary from 2–20 $\times 10^{-7}$ J cm^{-2} for highly soluble substances up to 50–150 $\times 10^{-7}$ J cm^{-2} for sparingly soluble compounds (Sohnel, 1982). The number of intermolecular interactions and their strength per lattice unit in protein crystals is considerably lower than for inorganic crystals. Protein crystals also contain vast amounts of solvent which can, in some cases, make up to 90% of the volume (McPherson, 1990). Thus, the difference in the nature of the molecular environment in solution and in the crystalline phase is considerably less for macromolecular crystals rather than for inorganic crystals. The work (*i.e.* interfacial free energy) to produce a surface unit of protein crystal should, therefore, also be correspondingly lower than for inorganic crystals.

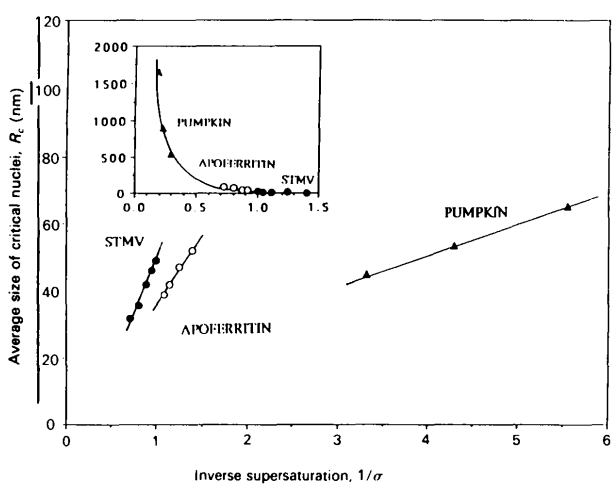

Fig. 7. The dependencies of the critical nuclear size R_c *versus* inverse supersaturation, $1/\sigma$, for pumpkin globulin, apoferritin and STMV crystallization. Corresponding values for interfacial free energies α and molar surface energies are: pumpkin globulin, $\alpha \simeq 6.1 \times 10^{-9}$ J cm^{-2} (3.3 kJ mol^{-1}); apoferritin, $\alpha \simeq 2.7 \times 10^{-9}$ J cm^{-2} (7.5 kJ mol^{-1}); STMV, $\alpha = 1.8 \times 10^{-9}$ J cm^{-2} (9.2 kJ mol^{-1}). Insert: the supersaturation dependency of the number of protein and virus particles comprising the critical nucleus.

The lowest (critical) supersaturation required for the appearance of visible crystals was estimated at $\sigma^* \simeq 0.9$, 0.7 and 0.1 for STMV, apoferritin and pumpkin seed globulin, respectively.

With the values of the interfacial free energies estimated above we can calculate the values of the potential barriers δF_c for formation of critical nuclei under conditions of moderate supersaturation where induction periods preceded the appearance of the critical nuclei. From (3), δF_c were calculated to be $\simeq 11.3$–46.0 kJ mol^{-1} in the supersaturation range $\sigma \simeq 0.15$–0.30, -37.6–62.7 kJ mol^{-1} ($\sigma \simeq 0.7$–0.9) and -20.9–52.7 kJ mol^{-1} ($\sigma \simeq 0.9$–1.4) for formation of critical nuclei in pumpkin globulin, apoferritin and STMV crystallization, respectively. The formation of a new crystalline phase requires breaking of bonds between protein and solvent molecules, diffusion of the protein molecules to the nuclear aggregate, incorporation in the aggregate and the formation of new bonds. The close values of δF_c for those macromolecular systems investigated so far show that qualitatively, and at least semiquantitatively, the energetics of formation of the crystalline phase appear to be very similar.

It should be noted that in the case of STMV crystallization we used a number of different inorganic precipitation agents. In all these cases we obtained quantitatively the same prenucleation and nucleation phenomena under the corresponding supersaturation conditions. This indicates that the mechanisms of the processes which took place in STMV solutions under supersaturation conditions were much the same and did not depend on precipitant. We intend to carry out crystallization experiments with organic precipitates and compare nucleation phenomena with those in the case of inorganic precipitates.

At supersaturation conditions higher than those when induction periods for formation of crystalline nuclei were obtained, immediately after incubation of protein solutions with precipitants, large aggregates with sizes in the range 300–500 nm appeared. These aggregates grew to μm sizes (Fig. 8) and shortly after visible microcrystals appeared in the solutions.

3.2.3. *Pumpkin seed globulin aggregation and dissociation kinetics: phase diagram for pumpkin seed globulin.* In the case when protein solubility depends upon temperature, for each combination of protein and precipitant concentrations there is an equilibrium temperature T_{eq} at which the chemical potentials of the protein molecule in the crystalline

and liquid phases are equal and there is eventually no exchange of protein molecules between the two phases. If pumpkin seed globulin solutions heated previously were cooled to below T_{eq}, crystallization took place (Fig. 9) and microcrystals were obtained in the solutions. Heating of the solutions containing microcrystals above T_{eq} always resulted in dissolution to monomers and small particles (Fig. 9). The rates of both aggregation and dissolution processes at the different temperatures depended upon the magnitude of the deviation (*i.e.* solution supersaturation) from the equilibrium temperature T_{eq}.

In order to determine the equilibrium conditions for the wide range of protein and precipitant concentrations and obtain a solubility diagram, the temperature-dependent aggregation and dissolution kinetics were investigated for 4.9–16 mg ml^{-1} pumpkin seed globulin solutions containing 1.5–7% NaCl.

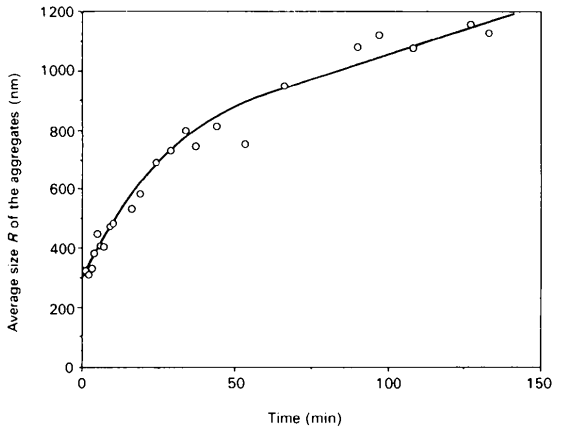

Fig. 8. Time dependencies of the average sizes of the aggregates R under solution supersaturations $\sigma \simeq 2.0$.

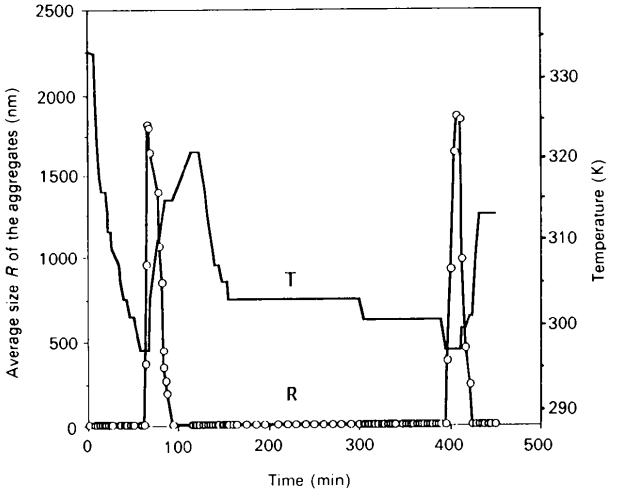

Fig. 9. A typical example of the temperature dependence of the aggregation–dissociation process for a pumpkin seed globulin solution (10 mg ml^{-1}, 2.9% NaCl). In the temperature range 301–333 K, only 8–10 nm clusters were obtained, while at T = 297 K aggregation proceeded to μm size aggregates.

For the investigation of aggregation kinetics we previously heated and kept samples for 5–10 min at 328–333 K. In this temperature range, corresponding to the undersaturated conditions, just pumpkin monomers and small clusters (as described in §3.2.1) existed in the solutions. Then samples were placed in a thermostat-controlled vat at the temperature corresponding to the supersaturated conditions and aggregation kinetics data were recorded. Before recording aggregation kinetics data at another temperature, samples were again kept at 328–333 K. Thus, each time aggregation kinetics data were recorded, only pumpkin globulin monomers and small clusters were present in the solutions at the beginning of the experiments.

For monitoring the dissociation kinetics at the different undersaturated conditions, a suspension of pumpkin globulin microcrystals was used. To do so, samples were maintained initially at 273–277 K for about 10–15 min. This resulted in the appearance of aggregates in the μm size range. Samples were then placed at the temperatures corresponding to undersaturated conditions and dissociation kinetics were recorded.

At equilibrium conditions (T_{eq}) no net dissociation of crystalline aggregates or aggregation of protein monomers and small clusters was observed. The equilibrium temperature T_{eq} was taken to be that corresponding to the midpoint between the highest temperature at which dissociation of microcrystals failed to occur and the highest temperature at which net aggregation of monomers and small clusters into larger species proceeded to occur.

Thus, for example, in 4.9 mg ml^{-1} pumpkin globulin solution containing 1.5% NaCl (Fig. 10), aggregation took place at a temperature just below 308 K (Fig. 10*a*). At 309 K and higher, no aggregation occurred. In the same protein sample containing microcrystals (Fig. 10*b*), complete dissociation took place at temperatures above 309 K, but not below 307 K. For this sample, therefore, the equilibrium temperature T_{eq} was taken to be ~308 K.

From the data on aggregation and dissociation kinetics for 4.9–16 mg ml^{-1} pumpkin globulin solutions containing 1–7% NaCl, the equilibrium temperatures T_{eq} were determined and a solubility diagram was obtained (Fig. 11). The solubility curve divides the entire temperature–precipitant concentration field (Fig. 11, solid line) into two regions corresponding to undersaturated and supersaturated states. From the experimental data presented in Fig. 11 the equilibrium temperature T_{eq} decreases from ~310–311 K (1% NaCl) to ~280–281 K (7% NaCl).

From our experimental data we obtained the temperature range where only aggregates with sizes in the range 200–400 nm appeared in relatively small amounts (usually less than 1% by mass) (Fig. 10). These aggregates never developed into microcrystals and their sizes actually did not increase through the entire course of the experiments, the longest experiment lasting about 10 d. However, we did not obtain dissociation in suspensions of microcrystals in the same temperature range. This indicates supersaturation conditions to be present, but below the level required for the formation of the critical nuclei, *i.e.* corresponding to the metastable zone.

Indeed, from (3) it follows that for a solution supersaturation of $\sigma \simeq 0.03$ (a third of critical supersaturation $\sigma^* \simeq 0.1$, §3.2.2), the size of a critical nucleus R_c should be ~ 300 nm. To form critical nuclei of $R_c \simeq 300$ nm, the system would have to overcome [see (3)] a potential barrier of $\delta F_c \simeq 3.3 \times 10^3$ kJ mol^{-1}, a highly improbable event. However, for supersaturation σ in the range ~ 0.15–0.30, the potential barrier δF_c is only ~ 12.5–50 kJ mol^{-1} (§3.2.2).

Note that for STMV crystallization at supersaturations less than ~ 0.7 (critical supersaturation $\simeq 0.9$) the sizes of critical nuclei should exceed ~ 85 nm, which are larger than those aggregates that appeared under the metastable conditions (§3.2.1).

Thus, the region of supersaturation for the pumpkin seed globulin, as also for STMV (§3.2.1) and most of the conventional systems, is divided into metastable and labile zones (Fig. 11). The metastable conditions usually existed within 1–2 K below the solubility curve (Fig. 11). At supersaturated conditions (temperatures lower than those corresponding to the metastable zone) aggregation proceeds rather quickly (Fig. 10) to yield μm size aggregates, and this is followed by the appearance of visible microcrystals.

3.2.4. *Amorphous precipitation.* Here we will describe the phenomena in STMV aggregation leading to amorphous precipitation. For these experiments we used highly monodisperse STMV samples, where just STMV monomers were present in the solutions and no small clusters were observed at undersaturated conditions. When these monodisperse STMV solutions were incubated with the same precipitants as those more polydisperse STMV solutions, the aggregation phenomena were completely different. In most cases an amorphous precipitate was obtained. In some cases the amorphous precipitate was accompanied by monoclinic STMV crystals.

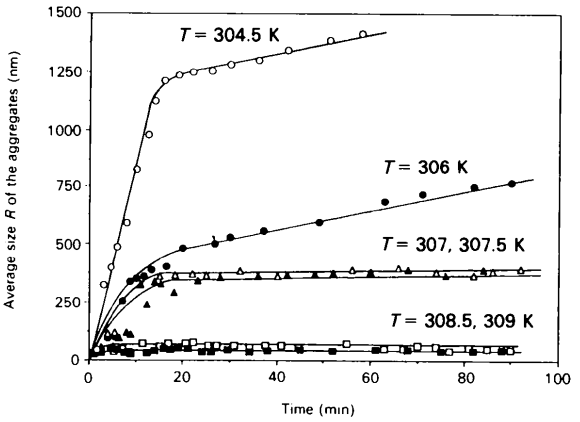

(*a*)

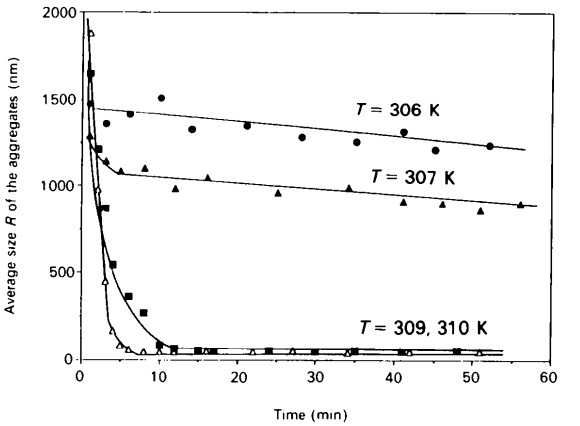

(*b*)

Fig. 10. The time dependencies of the average sizes of aggregates R, formed during the aggregation (*a*) and dissolution (*b*) processes at different temperatures for a 4.9 mg ml^{-1} protein, 1.5% NaCl pumpkin globulin solution.

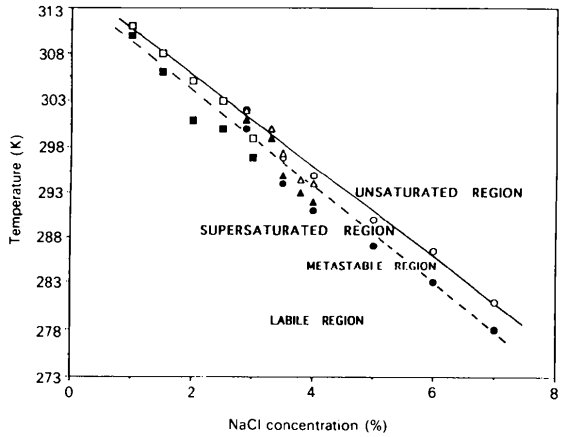

Fig. 11. Phase diagram for the 4.9–16 mg ml^{-1} pumpkin globulin solutions *versus* NaCl concentrations. ○, ● 16 mg ml^{-1}; □, ■ 4.9 mg ml^{-1}; △, ▲ 10 mg ml^{-1}. The solid line (open symbols) divides the entire region into supersaturated and undersaturated zones. The dashed line (filled-in symbols) corresponds to the metastable zone.

Qualitatively, the aggregation pathways were the same when we used different precipitates: 0.25–1.2 *M* lithium sulfate, 20–30% saturated ammonium sulfate or 1.0–1.4 *M* ammonium phosphate (Figs. 12–15). In all cases two stages were seen during the aggregation process leading to amorphous aggregates with sizes in the μm range.

During the first stage the average sizes of the aggregates slowly increased up to 90–120 nm. In different experiments, depending upon the degree of solution supersaturation, this took from ~15 h to just ~1 h (Figs. 12–15). The rates of incorporation of STMV particles were low and corresponded to the addition of approximately 1–2 STMV every 3–5 min (Fig. 16).

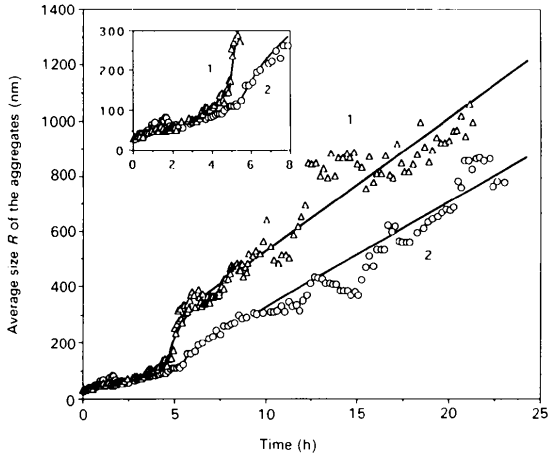

Fig. 12. Time dependencies of the average size of aggregates *R* during amorphous precipitation. Solution supersaturations σ: (1) 0.6 (3.6 mg ml^{-1} STMV incubated with 0.5 *M* Li sulfate); (2) 1.9 (3.6 mg ml^{-1} STMV incubated with 1.2 *M* Li sulfate). Insert: details of the initial periods of aggregation.

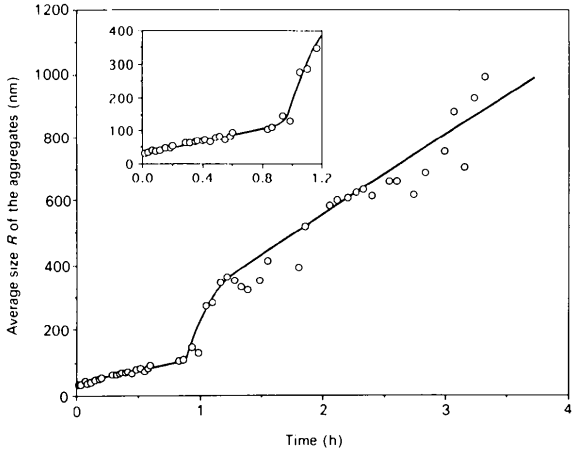

Fig. 13. Time dependence of the averge size of aggregates *R* during amorphous precipitation. Solution supersaturation $\sigma \simeq 0.7$ (1.8 mg ml^{-1} STMV incubated with 1.5 *M* ammonium phosphate). Insert: details of the initial period of aggregation.

At the lower value of supersaturation when 1.8 mg ml^{-1} was incubated with 0.1 *M* Li sulfate, we obtained over 200 h a very slow increase in aggregate sizes up 200–300 nm (Fig. 15). After 6–8 weeks no visible amorphous precipitant was present in the solution, with the aggregates still being in the 200–400 nm range. The rate of incorporation of the STMV particles during the aggregation process was very low (Fig. 16), corresponding to incorporation of just one STMV in 15 min.

Aggregates with sizes in the range 90–120 nm were likely to correspond to those of critical size, since after their appearance in solution a rather quick aggregation (corresponding to the second stage mentioned above) took place and aggregates with sizes in μm range appeared (Figs. 12–15). This was followed

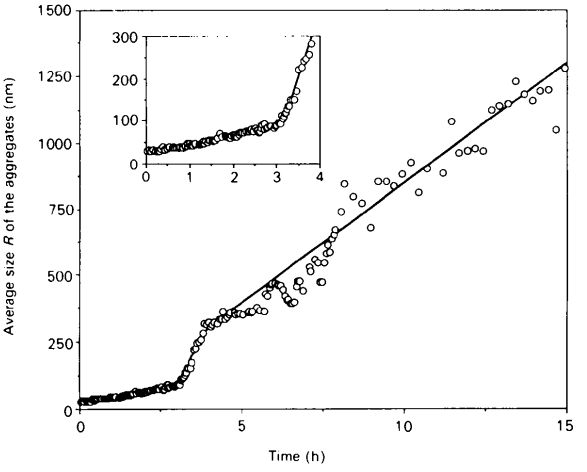

Fig. 14. Time dependence of the average size of aggregates *R* during amorphous precipitation. Solution supersaturation $\sigma \simeq 1.2$ (3.6 mg ml^{-1} STMV incubated with 20% saturated ammonium sulfate). Insert: details of the initial period of aggregation.

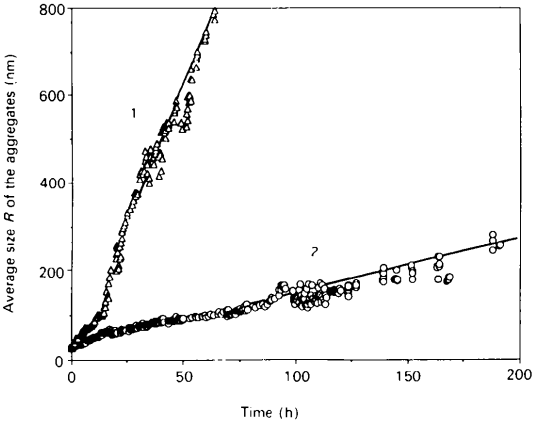

Fig. 15. Time dependencies of the average sizes *R* in 1.8 mg ml^{-1} STMV solutions incubated with: (1) 0.25 *M* lithium sulfate ($\sigma \simeq 0.4$); (2) 0.1 *M* lithium sulfate.

by the appearance of the visible amorphous precipitate. Note that in our previous experiments on STMV precipitation, when ethanol was used as a precipitant (Malkin & McPherson, 1993*a*), and amorphous precipitation of ferritin (Malkin & McPherson, 1993*b*) we obtained qualitatively the same aggregation pathways as those described here.

It is interesting to mention that at low supersaturation conditions when we never observed the appearance of visible amorphous precipitate (which probably corresponded to the metastable conditions), continuous aggregation took place over the entire experiment (Fig. 17). This was completely different in comparison to the aggregation phenomena which took place under crystallization conditions corresponding to the metastable zone (§3.2.1). Under those conditions (Fig. 17) we did not obtain any significant increase in the aggregate sizes over long periods of time. The size of aggregates actually fluctuated without increase: both aggregation and dissociation took place. Qualitatively, the same differences were obtained under conditions when critical nuclei were formed. Thus, in the case of crystallization the formation of critical nuclei and further aggregation took place due to the fluctuation of the free energy of the aggregates. Preceding formation of the crystalline critical nuclei, there were again no increases in the sizes of prenucleation aggregates (Figs. 4–6), whereas in the case of amorphous precipitation a slow increase, up to 90–120 nm, took place as described above (Figs. 12–15).

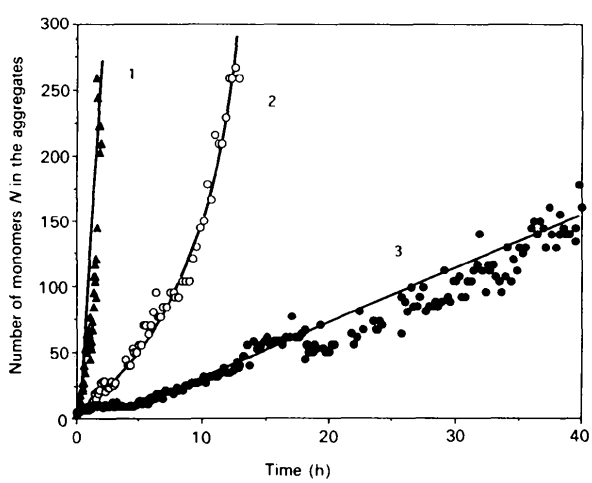

Fig. 16. Time dependencies of the numbers of STMV monomers in the aggregates formed in the solutions when: (1) 3.6 mg ml^{-1} STMV was incubated with 0.5 *M* lithium sulfate; (2) 1.8 mg ml^{-1} STMV was incubated with 0.25 *M* lithium sulfate; (3) 1.8 mg ml^{-1} STMV was incubated with 0.1 *M* lithium sulfate. The corresponding incorporation rates are ~1.8 STMV monomer min^{-1}; 1 STMV monomer min^{-1}; and 1 STMV monomer per 15 min.

It is not clear at this point why relatively sharp increases in the aggregate sizes usually took place after an appearance in the solutions of 90–120 nm aggregates (Figs. 12–15). During the first stages of the aggregation process leading to an amorphous precipitate we clearly obtained two peaks in the PSD corresponding to STMV monomers and to the aggregates of size 30 nm and higher, which were formed since supersaturation conditions were created. There were no small clusters with sizes in the range 19–30 nm, as described for STMV solutions, which provided crystals rather than an amorphous precipitate (§3.1). Thus, aggregation leading to the amorphous precipitate probably proceeded through attachment of STMV monomers, which resulted in a rather slow kinetics, whereas under crystallization conditions small clusters which clearly existed in the solutions could play the role of building units. Probably, in the course of amorphous precipitation when larger 90–120 nm aggregates appeared in the solutions, they aggregate with each other resulting in a quicker kinetics.

It is interesting to indicate here that under the same precipitation conditions for monodispersive STMV solutions using vapor diffusion methods (in which supersaturated conditions established more slowly) instead of batch methods as described above, we repeatedly obtained monoclinic STMV crystals instead of typical orthorombic STMV crystals. Thus, different aggregation pathways, where presumably in one case attachment of monomers to the clusters and in another case cluster–cluster aggregation took place, lead to different crystal forms.

At this point the results described here for the aggregation phenomena leading to amorphous precipitation are much more qualitative than those

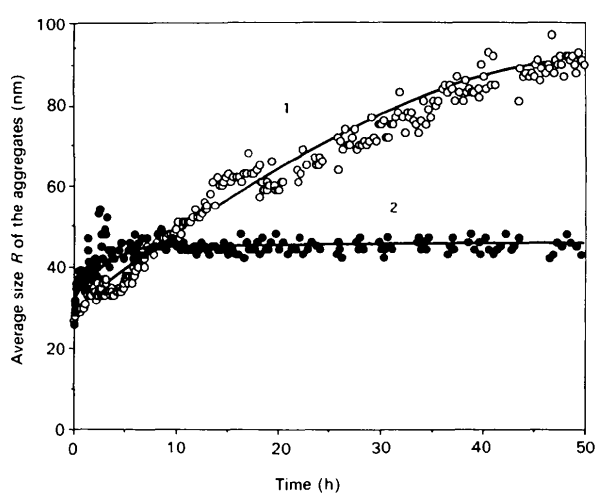

Fig. 17. Time dependencies of the average sizes *R* of the aggregates formed under metastable conditions: (1) amorphous precipitation conditions, (2) crystallization conditions.

described for crystallization conditions. We plan to perform further experiments on amorphous precipitation in macromolecular systems using both organic and inorganic precipitants. We believe that the results of such experiments could be important since they will help to develop a criteria of determination of the ultimate fate of the aggregation process on early nucleation stages.

4. Concluding remarks

(1) Quasi-elastic light scattering was applied to the investigation of nucleation phenomena, postnucleation events and dissociation in ensembles of both crystalline and amorphous aggregates of satellite tobacco mosaic virus (STMV), ferritin, apoferritin and pumpkin seed globulin.

(2) The metastable region for STMV and pumpkin seed globulin crystallization was obtained. Under these conditions aggregation took place, but the sizes of the aggregates never achieved those required for critical nuclei. Thus, at these supersaturations no crystallization took place.

(3) For all macromolecular systems investigated in this work so far. the supersaturation dependencies of the critical nuclei supportive of stable crystal growth were obtained. The interfacial free energies were estimated from this data to be in range $1.8–6.1 \times 10^{-9}$ J cm^{-2}. The potential barriers for the formation of critical nuclei, under supersaturation conditions of moderate supersaturation, were estimated to be in range 8–50 kJ mol^{-1}.

(4) For pumpkin seed globulin, data on the temperature dependence of protein solubility *versus* precipitant concentration, based on aggregation and dissolution kinetics, were obtained.

(5) The significant differences in the aggregation pathways leading both to formation of an amorphous precipitate and crystals were described.

This research was supported by grants from NASA and the NSF. The authors wish to thank Ms J. Cheung for her help and isolation and purification of pumpkin seed globulin.

References

BERNE, B. J. & PECORA, R. (1976). *Dynamic Light Scattering*, p. 376. New York: John Wiley.

BISHOP, J. B., FREDERICKS, W. J., HOWARD, S. B. & SAWADA, T. (1992). *J. Cryst. Growth*, **122**, 41–49.

CARTER, C. W. JR, BALDWIN, E. T. & FRICK, L. (1988). *J. Cryst. Growth*, **90**, 60–73.

CHERNOV, A. A. (1984). *Modern Crystallography* III: *Crystal Growth*, Springer Series in Solid State Sciences, Vol. 36. Berlin: Springer.

CUMMINS, P. G. & STAPLES, E. J. (1987). *Langmuir*, **3**, 1109–1113.

DURBIN, S. D. & FEHER, G. (1990). *J. Mol. Biol.* **212**, 763–774.

HARA, I., WADA, K., WAKABAYASHI, S. & MATSUBARA, H. (1976). *Plant Cell Physiol.* **17**, 799–814.

HARRISON, P. M. (1959). *J. Mol. Biol.* **1**, 69–80.

KADIMA, W., MCPHERSON, A., DUNN, M. F. & JURNAK, F. (1991). *J. Cryst. Growth*, **110**, 188–194.

KAM, F., SHORE, H. B. & FEHER, G. (1978). *J. Mol. Biol.* **123**, 539–555.

KOSZELAK, S., DODDS, J. A. & MCPHERSON, A. (1989). *J. Mol. Biol.* **208**, 323–325.

LARSON, S. B., KOSZELAK, S., DAY, J., GREENWOOD, A. & MCPHERSON, A. (1993*a*). *Nature (London)*, **361**, 179–182.

LARSON, S. B., KOSZELAK, S., DAY, J., GREENWOOD, A. & MCPHERSON, A. (1993*b*). *J. Mol. Biol.* **231**, 375–391.

LORBER, B., SKOURI, M., MUNCH, J. P. & GIEGÉ, R. (1993). *J. Cryst. Growth*, **128**, 1203–1211.

MCPHERSON, A. (1990). *Eur. J. Biochem.* **198**, 1–23.

MALKIN, A. J., CHEUNG, J. & MCPHERSON, A. (1993). *J. Cryst. Growth*, **126**, 544–554.

MALKIN, A. J. & MCPHERSON, A. (1993*a*). *J. Cryst. Growth*, **126**, 555–564.

MALKIN, A. J. & MCPHERSON, A. (1993*b*). *J. Cryst. Growth*, **128**, 1232–1235.

MALKIN, A. J. & MCPHERSON, A. (1993*c*). *J. Cryst. Growth*, **133**, 29–37.

MIKOL, V., HIRSH, E. & GIEGÉ, R. (1990). *J. Mol. Biol.* **213**, 187–195.

PECORA, R. (1985). *Light Scattering: Application of Photon Correlation Spectroscopy*. New York: Plenum Press.

SOHNEL, O. (1982). *J. Cryst. Growth*, **57**, 101–108.

TREFFRY, A. & HARRISON, P. M. (1978). *Biochem. J.* **171**, 313–324.

VALVERDE, R. A. & DODDS, J. A. (1987). *J. Gen. Virol.* **68**, 965–972.

WILSON, W. W. (1990). *Methods: a Companion to Methods in Enzymology*, Vol. 1, pp. 110–117. New York: Academic Press.